Supporting Information

Promoted Electroreduction of CO_2 with Oxygen Vacancies on Plasma-Activated SnO_x/Carbon Foam Monolithic Electrode

Hongqiang Li [1], Nan Xiao [1] *, Yuwei Wang [1], Chang Liu [3], Shengji Zhang [1], Huihui Zhang [1], Jinpeng Bai [1], Jian Xiao [1], Chen Li [1], Zhen Guo [1], Shijia Zhao [1], and Jieshan Qiu[1, 2] *

[1] *State Key Lab of Fine Chemicals, School of Chemical Engineering, Liaoning Key Lab for Energy Materials and Chemical Engineering, PSU-DUT Joint Center for Energy Research, Dalian University of Technology, Dalian 116024, China.*

[2] *College of Chemical Engineering, Beijing University of Chemical Technology, Beijing 100029, China*

[3] *Institute of Organic Luminescent Materials (IOLM), College of Chemistry, Liaoning University, Shenyang 110036, China*

E-mail: nxiao@dlut.edu.cn (N. Xiao) jqiu@dlut.edu.cn (J. Qiu)

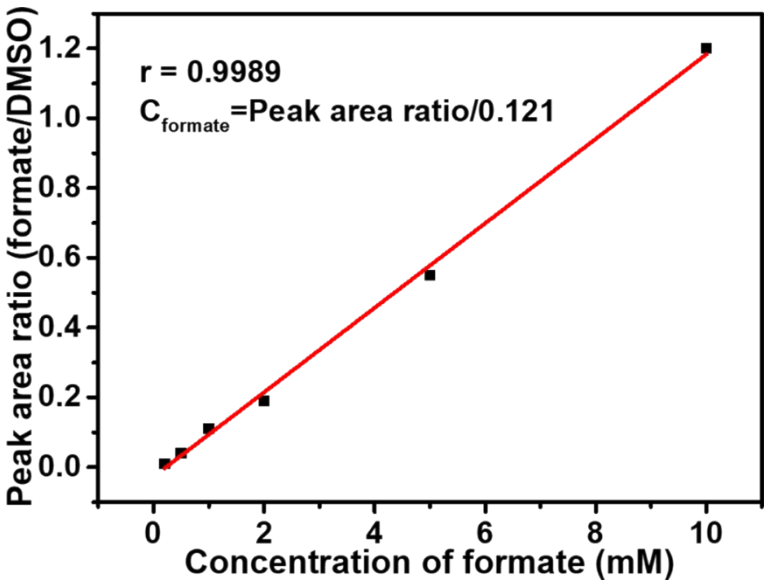

Figure S1. Linear relationship between the formate concentration and relative peak area ratio (formate/DMSO).

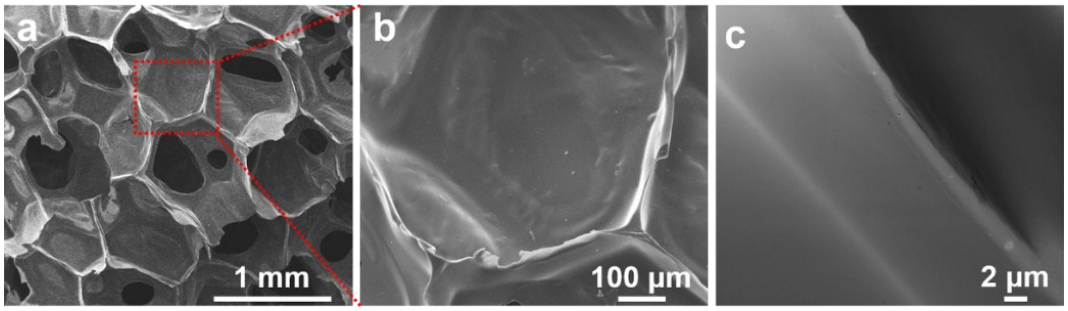

Figure S2. (a) Low-magnification and (b, c) high-magnification FE-SEM images of pristine carbon foam.

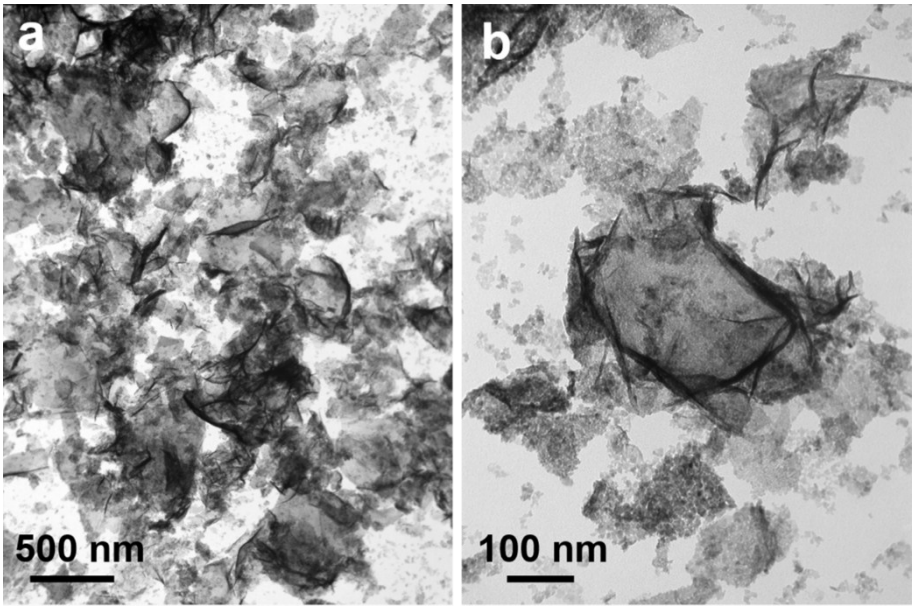

Figure S3. TEM images of pristine SnO_2 nanosheets.

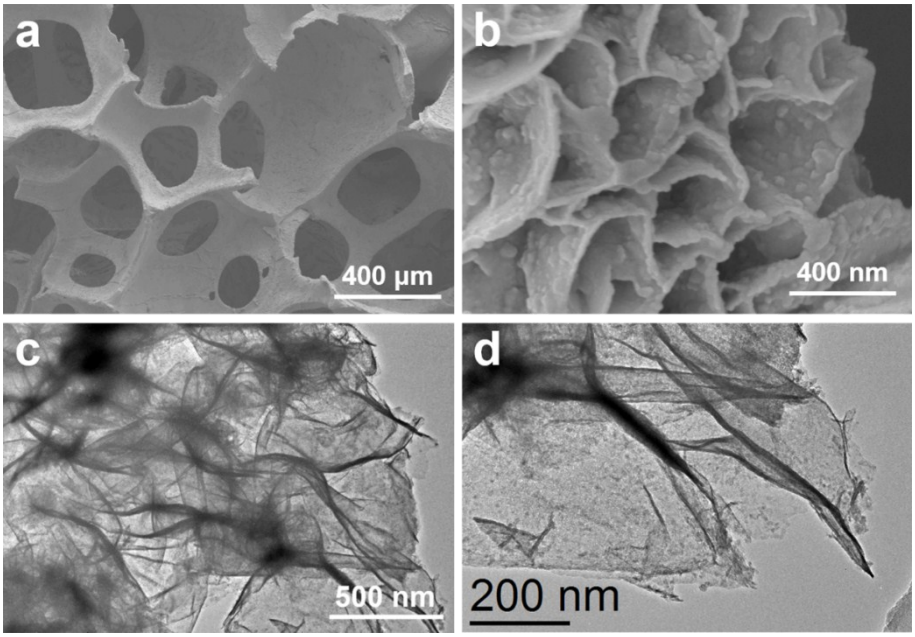

Figure S4. (a) Low-magnification and (b) high-magnification FE-SEM images of V_O-SnO_x/CF sample. (c, d) TEM images of V_O-SnO_x/CF sample.

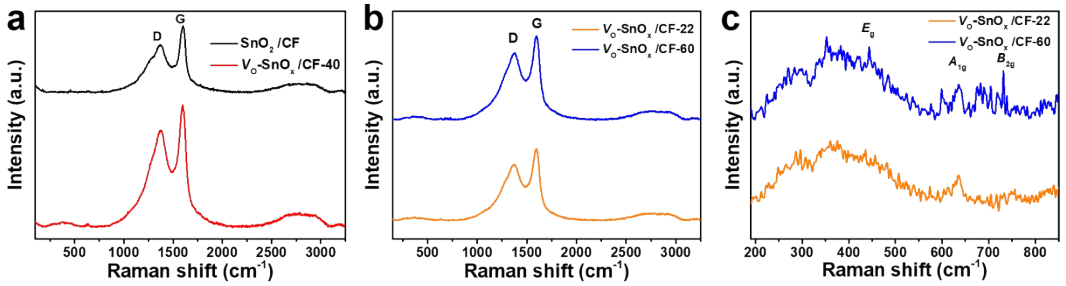

Figure S5. (a) Raman spectra of pristine SnO_2/CF and V_O-SnO_x/CF-40. (b) Raman spectra of V_O-SnO_x/CF-22 and V_O-SnO_x/CF-60. (c) High-magnification Raman spectra of V_O-SnO_x/CF-22 and V_O-SnO_x/CF-60.

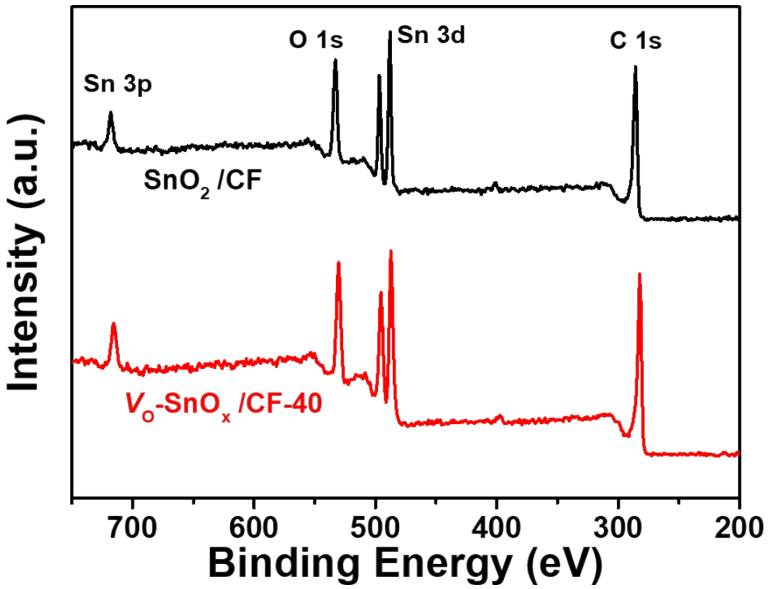

Figure S6. XPS spectra of pristine SnO_2/CF and V_O-SnO_2/CF-40 samples.

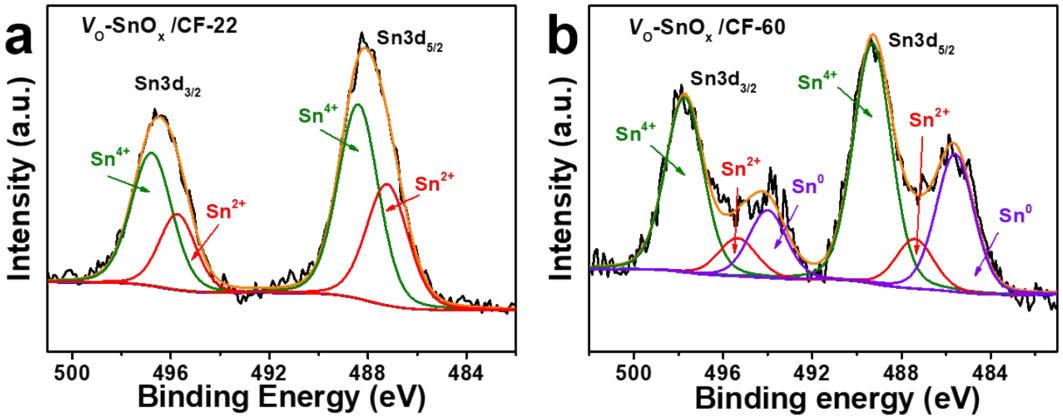

Figure S7. High-resolution XPS spectra of Sn 3d for V_O-SnO$_x$/CF-22 (a) and V_O-SnO$_x$/CF-60 (b).

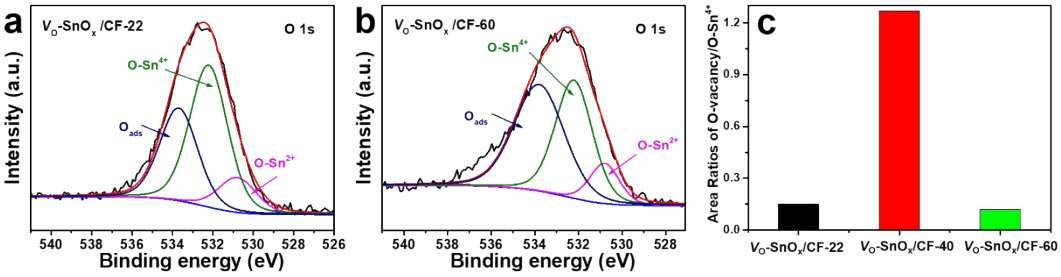

Figure S8. XPS spectra of O 1s for V_O-SnO_2/CF-22 (a) and V_O-SnO_2/CF-60 (b), the calculated ratio of integral areas for the peaks of O-vacancy and O-Sn^{4+} in O 1s XPS spectra of different *V*o-SnO_2/CFs (c).

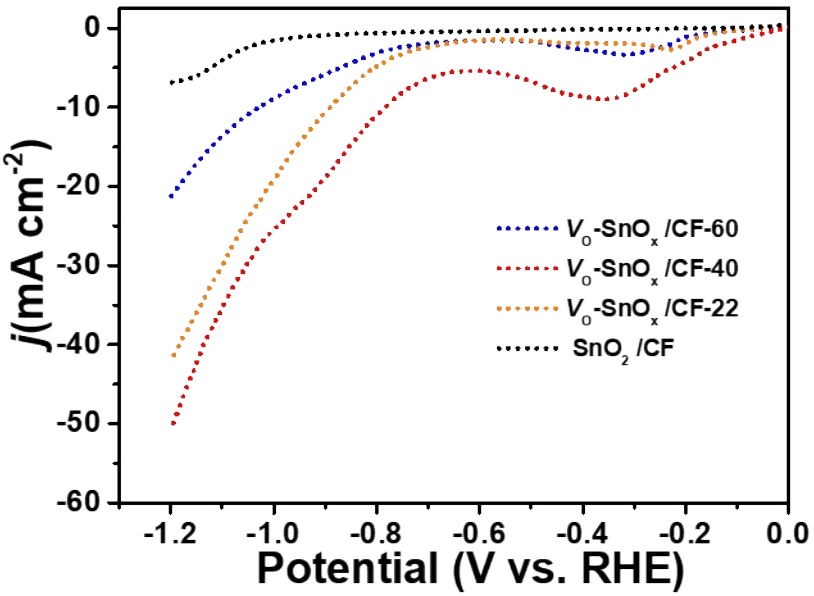

Figure S9. Linear sweep voltammetry curves of the prepared electrodes in Ar-saturated 0.1 M $KHCO_3$ aqueous solution at a scan rate of 20 mV s^{-1}.

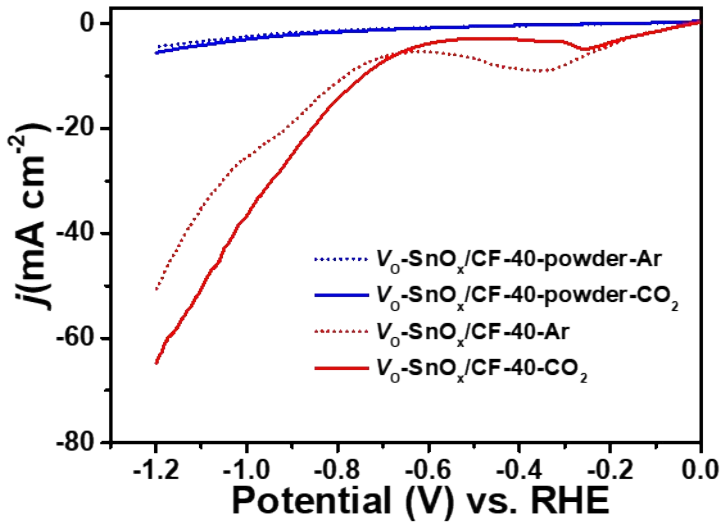

Figure S10. Linear sweep voltammetry curves of the V_O-SnO_x/CF-40 powder and the V_O-SnO_x/CF-40 monolithic electrode in Ar- and CO_2-saturated 0.1 M $KHCO_3$ aqueous solution at a scan rate of 20 mV s^{-1}.

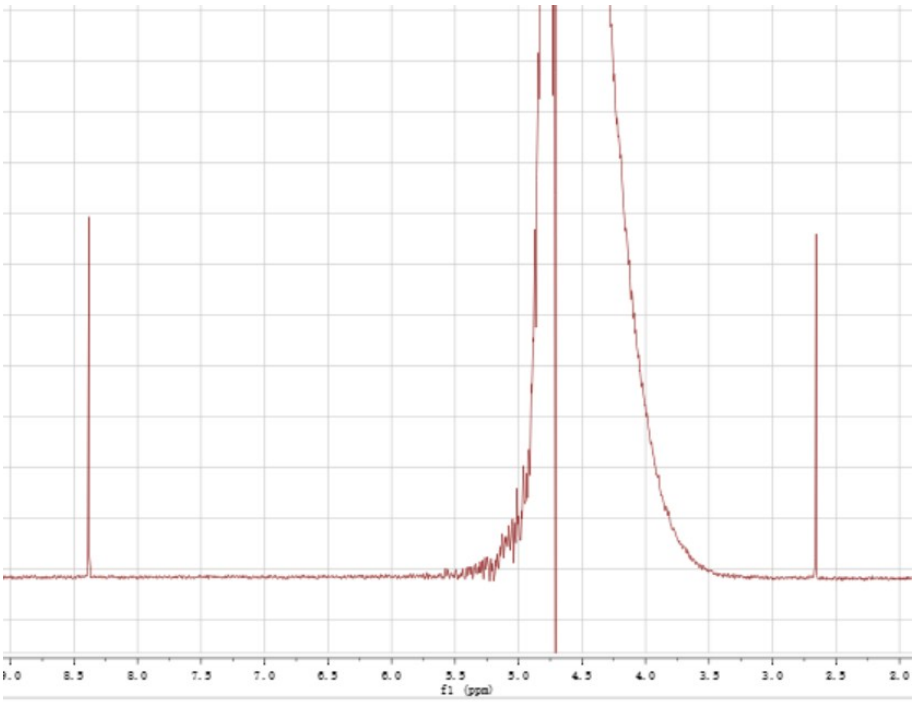

Figure S11. 1H-NMR spectrum of 0.1 M $KHCO_3$ electrolyte after 2 h electrolysis at -1.0 V (vs. RHE) of the V_O-SnO_x/CF-40.

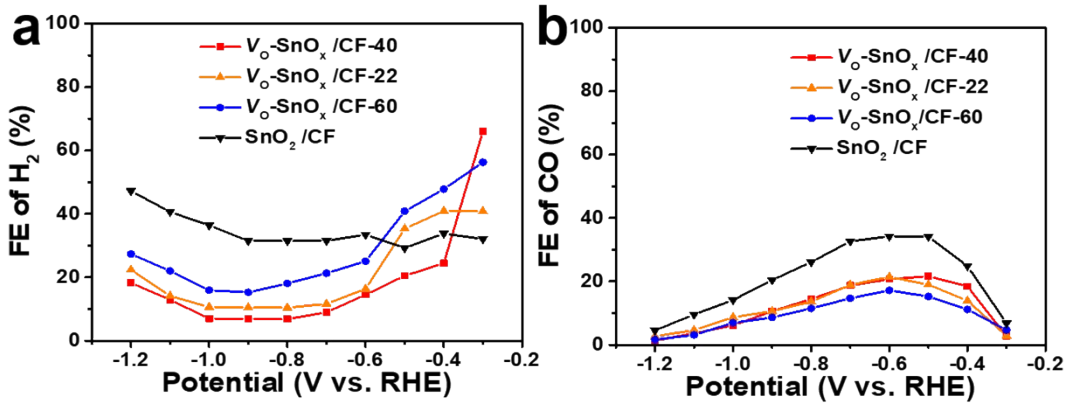

Figure S12. FE of H_2 (a) and CO (b) for various electrodes at different electrolytic potentials.

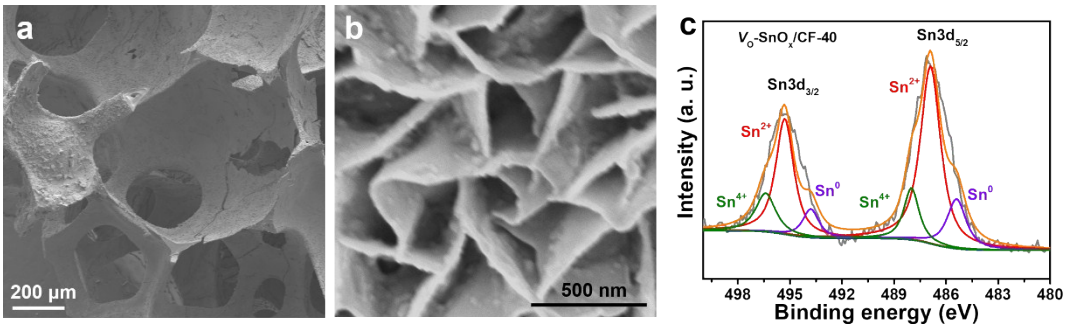

Figure S13. Physical characterization of V_O-SnO$_x$/CF-40 after 8 h CO_2 reduction. (a) low-resolution FESEM image, (b) high-resolution FESEM image, (c) XPS spectrum of Sn 3d.

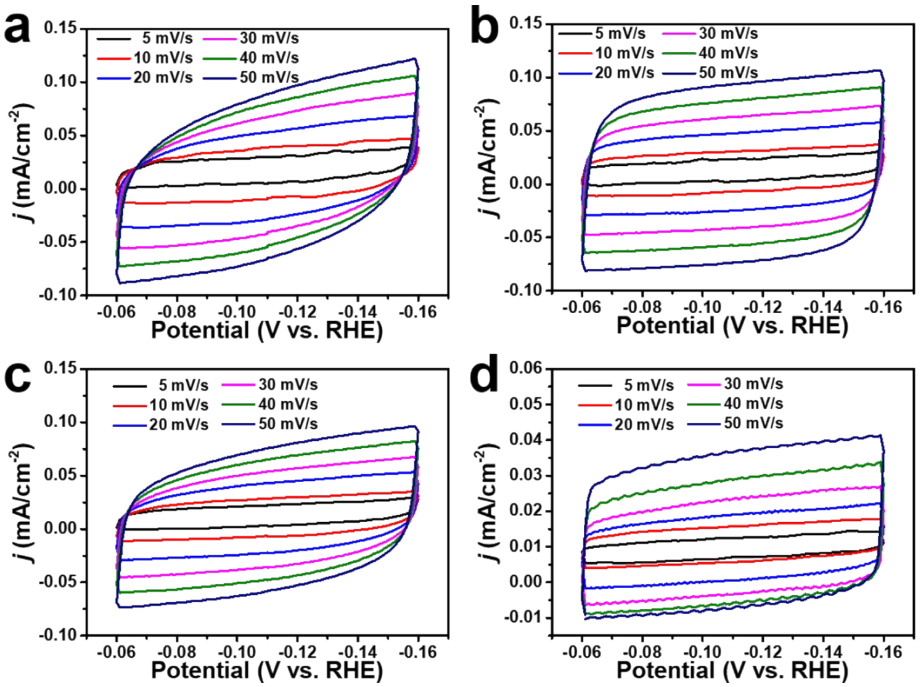

Figure S14. Cyclic voltammograms at the range of -0.06 to -0.16 V vs. RHE with different scan rates (5, 10, 20, 30, 40, and 50 mV s^{-1}) for V_O-SnO_x/CF-22 (a), V_O-SnO_x/CF-40 (b), V_O-SnO_x/CF-60 (c), and pristine SnO_2/CF (d).

Supplementary Note 1:

Determination of electrochemically active surface area (ECSA).

The ECSAs of the electrodes were determined by the measurement of the double-layer capacitance (C_{dl}). To measure the C_{dl}, Cyclic voltammograms were measured in a non-faradaic region (potential range between -0.06 and -0.16 V vs. RHE) of the voltammogram at varied scan rates (5, 10, 20, 30, 40, and 50 mV s^{-1}). The capacitive currents of Δj (j_a-j_c)@-0.11 V/2 (where j_a and j_c were the anodic and cathodic current densities, respectively) are plotted as a function of the CV scan rates. These data were fitted to a line. The slope of the line is the double layer capacitance (C_{dl}), which is proportional to the ECSA of electrodes.

To facilitate the comparison of ECSA data between different electrodes, the monolithic electrodes were ground to powder for ECSA testing. The powder was then dripped onto the surface of a glassy carbon electrode (S = 0.196 cm^2) for CV testing at varied scan rates (5, 10, 20, 30, 40, and 50 mV s^{-1}).

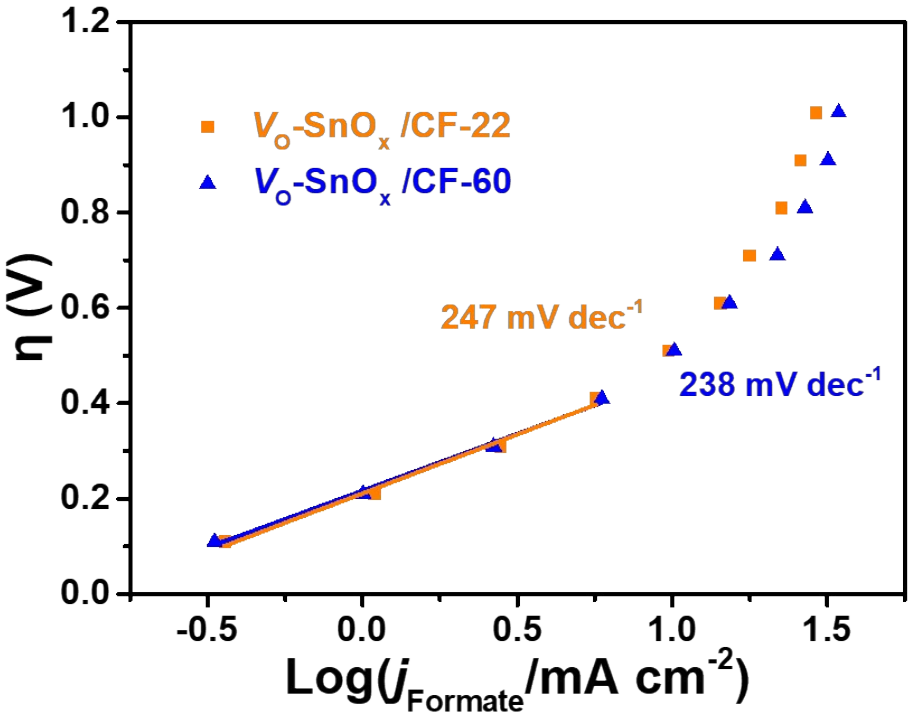

Figure S15. Tafel plots for V_O-SnO_2/CF-22 and V_O-SnO_2/CF-60.

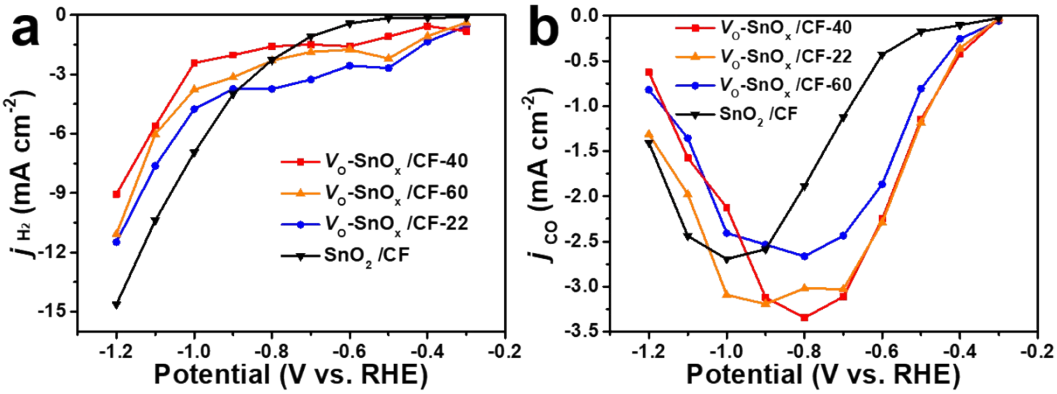

Figure S16. Partial current density of H_2 (a) and CO (b) for various electrodes at different electrolytic potentials.

Supplementary Note 2:

The partial current densities at different potentials were calculated by multiplying the overall geometric current densities and the corresponding faradic efficiencies.